Eur. Phys. J. D **9**, 487–490 (1999)

THE EUROPEAN PHYSICAL JOURNAL D

EDP Sciences

Quantum dots in magnetic fields: Unrestricted symmetries in the current spin-density functional formalism

M. Koskinen[1,a], J. Kolehmainen[1], S.M. Reimann[1], J. Toivanen[2], and M. Manninen

[1] Department of Physics, University of Jyväskylä, FIN-40351 Jyväskylä, Finland
[2] Department of Mathematics, University of Jyväskylä, FIN-40351 Jyväskylä, Finland

Received: 1 September 1998 / Received in final form: 21 October 1998

Abstract. We apply the current spin-density functional formalism (CSDFT) of Vignale and Rasolt to two-dimensional quantum dots in magnetic fields. Avoiding any spatial symmetry restrictions of the solutions, we find that a broken rotational symmetry of the electronic charge density can occur in high magnetic fields.

PACS. 71. Electronic structure – 73.20.Dx Electron states in low-dimensional structures – 85.30.Vw Low-dimensional quantum devices

1 Introduction

Several experiments on lateral or vertical quantum dots (i.e., small semiconductor nanostructures; see [1] for a review) have been performed in large magnetic fields with the aim of exploring the transition from the quantum Hall to the fractional quantum Hall regime of the confined two-dimensional electron gas [2–4]. Only vertical quantum dots containing very few electrons could be experimentally realized by Tarucha *et al.* [5]: Measurements in zero and weak magnetic fields demonstrated the validity of a shell model and Hund's rules. More recent experimental work [6] focuses on parabolic quantum dots at filling factors $\nu \leq 1$, and we thus found it worthwhile to extend the spin-density formalism applied to circular quantum dots in our earlier work [7] to the inclusion of homogeneous magnetic fields by applying the so-called current spin-density functional theory (CSDFT) of Vignale and Rasolt [8], which provides a method for describing interacting electrons in a gauge field. In these proceedings, we report results of our calculations in the polarized regime, showing that in large magnetic fields, broken-symmetry solutions for the charge density [9] may exist. A comparison to experimental results and the effect of magnetic fields on spin- and charge-density waves and singlet–triplet oscillations in weaker magnetic fields will be published elsewhere. Here, we concentrate on giving a short summary of our computational method within CSDFT for the case of unrestricted symmetry. We then discuss the example of a circular quantum dot with 10 electrons in strong magnetic fields.

[a] e-mail: koskinen@phys.jyu.fl

2 Current spin-density functional formalism

We employ the current- and spin-density functional formalism (CSDFT) [8] to calculate the electronic structure of quantum dots in an external magnetic field. We refer to the original work of Vignale and Rasolt [8] for a detailed description of CSDFT.

Consider now N interacting electrons that are restricted to move in the plane $\mathbf{r} = (x, y)$ in an external scalar potential $V(\mathbf{r})$ and a magnetic field $\mathbf{B} = B\mathbf{e}_z$ perpendicular to the x, y plane. In the symmetric gauge, the external vector potential acting on the electrons is thus $\mathbf{A}(\mathbf{r}) = B/2(-y, x)$. After a local approximation for the exchange-correlation energy is made, the total energy of the system is written as a functional of single-particle states $\Psi_{i\delta}$ with occupation numbers $f_{i\delta}$, where i labels the eigenstates within spin $\delta = (\uparrow, \downarrow)$:

$$\begin{aligned} E[\Psi_{i\delta}] = & \sum_{i\delta} f_{i\delta} \, \langle \Psi_{i\delta} \mid -\frac{\hbar^2 \nabla^2}{2m^*} \mid \Psi_{i\delta} \rangle \\ & + \frac{1}{2} \frac{e^2}{4\pi\epsilon_0 \epsilon} \int\int \mathrm{d}\mathbf{r} \, \mathrm{d}\mathbf{r}' \, \frac{n(\mathbf{r}) n(\mathbf{r}')}{\mid \mathbf{r} - \mathbf{r}' \mid} \\ & + \int \mathrm{d}\mathbf{r} \, n(\mathbf{r}) e_{\mathrm{xc}}[n_\delta(\mathbf{r}), \gamma(\mathbf{r})] \\ & + \int \mathrm{d}\mathbf{r} \, n(\mathbf{r}) V(\mathbf{r}) \\ & + \frac{1}{2} g^* \mu_{\mathrm{B}} B \int \mathrm{d}\mathbf{r} \, [n_\uparrow(\mathbf{r}) - n_\downarrow(\mathbf{r})] \\ & + e \int \mathrm{d}\mathbf{r} \, \mathbf{j}_p(\mathbf{r}) \cdot \mathbf{A}(\mathbf{r}) \\ & + \frac{e^2}{2m^*} \int \mathrm{d}\mathbf{r} \, n(\mathbf{r}) A(\mathbf{r})^2 \, . \end{aligned} \tag{1}$$

Here e is the (absolute) electron charge, g^* a reduced Landé g factor, and $\mu_{\rm B}$ the Bohr magneton. The total particle density is the sum of up-spin and down-spin density,

$$n(\mathbf{r}) = n_\uparrow(\mathbf{r}) + n_\downarrow(\mathbf{r}) \;, \tag{2}$$

$$n_\delta(\mathbf{r}) = \sum_i f_{i\delta} \mid \Psi_{i\delta}(\mathbf{r}) \mid^2 \;. \tag{3}$$

The paramagnetic current density $\mathbf{j}_p(\mathbf{r})$ is defined as

$$\mathbf{j}_p(\mathbf{r}) = -\frac{i\hbar}{2m^*} \sum_{i\delta} f_{i\delta} [\Psi^*_{i\delta}(\mathbf{r}) \nabla \Psi_{i\delta}(\mathbf{r}) - \Psi_{i\delta}(\mathbf{r}) \nabla \Psi^*_{i\delta}(\mathbf{r})] \;. \tag{4}$$

The thermal occupation numbers

$$f_{i\delta} = \frac{1}{1 + \exp[(\varepsilon_{i\delta} - \mu)/k_{\rm B}T]} \tag{5}$$

with chemical potential μ (which is adjusted on each iteration step to preserve the total electron number) and single-particle eigenenergies $\varepsilon_{i\delta}$ allow a partial occupation of levels at the Fermi surface for better convergence. This was found useful when, during the self-consistent iteration of the Kohn–Sham equations, the energy levels around the Fermi surface came very close in energy. After convergence is first reached for finite temperature, usually the Fermi surface is nondegenerate. In a second step, the temperature can then be dropped to zero, and finally, convergence of the zero-temperature solution can be obtained.

The functional (1) is formally equivalent to the Hartree energy, plus an extra exchange-correlation contribution. This takes into account that the true ground state of the system is not a product of single-particle eigenstates, but an antisymmetric many-body wave function of more complicated structure. In the limit of infinite homogeneous system the functional (1) becomes exact and the wave functions $\Psi_{i\delta}$ become pure Landau levels. Naturally, detailed many-body calculations for the bulk are necessary for one to obtain $e_{\rm xc}$ as a function of the electron spin-density n_δ and the strength of the external magnetic field B.

However, the first three terms of (1) describe the energy expectation value of the internal Hamiltonian of electrons and should not contain *a priori* any references to the external field. The exchange-correlation energy $e_{\rm xc}$ for the bulk depends on the field B, but this is only a consequence of the fact that the external field changes the internal structure of the wave function. It turns out that it is actually the vorticity

$$\gamma(\mathbf{r}) = \nabla \times \frac{\mathbf{j}_p(\mathbf{r})}{n(\mathbf{r})}\bigg|_z \tag{6}$$

of the wave function which is responsible for changes in $e_{\rm xc}$. It can be related to the external field B via the real current

$$\mathbf{j}(\mathbf{r}) = \mathbf{j}_p(\mathbf{r}) + \frac{e}{m^*}\mathbf{A}(\mathbf{r}) n(\mathbf{r}) \;. \tag{7}$$

For the homogeneous bulk, $\mathbf{j}(\mathbf{r}) = 0$. Dividing (7) by the density n and taking the cross product ($\mathbf{B} = \nabla \times \mathbf{A}$) gives

$$\nabla \times (\mathbf{j}_p(\mathbf{r})/n(\mathbf{r})) = -\frac{e}{m^*}\,\mathbf{B} \;. \tag{8}$$

Thus, when using the interpolation formulas for $e_{\rm xc}$ in CSDFT, one replaces the external field

$$B \;\longrightarrow\; \frac{m^*}{e} \mid \gamma(\mathbf{r}) \mid \;. \tag{9}$$

To minimize the total energy of the system, a functional derivative of $E[\Psi_{i\delta}]$ is taken with respect to $\Psi^*_{i\delta}$, the constraint of the $\Psi_{i\delta}$ being normalized is applied. The resulting self-consistent one-electron equation is

$$\left[\frac{\mathbf{p}^2}{2m^*} + \frac{e}{2m^*}\left(\mathbf{p}\cdot\boldsymbol{\mathcal{A}}(\mathbf{r}) \;+\; \boldsymbol{\mathcal{A}}(\mathbf{r})\cdot\mathbf{p}\right) + \mathcal{V}_\delta(\mathbf{r})\right] \Psi_{i\delta} = \varepsilon_{i\delta}\Psi_{i\delta} \tag{10}$$

where

$$\mathcal{V}_\delta(\mathbf{r}) = \frac{e^2}{2m^*}A(\mathbf{r})^2 + V_\delta(\mathbf{r}) + V_H(\mathbf{r}) + V_{{\rm xc}\delta}(\mathbf{r}) \;,$$

and

$$\begin{aligned}
\mathbf{p} &= -i\hbar\nabla \;, \qquad \boldsymbol{\mathcal{A}} = \mathbf{A} + \mathbf{A}_{\rm xc} \;, \\
e\mathbf{A}_{\rm xc} &= \frac{1}{n}\left\{\frac{\partial}{\partial y}\frac{\partial[n e_{\rm xc}(n_\delta,\gamma)]}{\partial\gamma} \;, -\frac{\partial}{\partial x}\frac{\partial[n e_{\rm xc}(n_\delta,\gamma)]}{\partial\gamma}\right\} \;, \\
V_{\uparrow,\downarrow} &= V \pm \frac{1}{2}g^*\mu_{\rm B}B \;, \\
V_H &= \frac{e^2}{4\pi\epsilon_0\epsilon}\int {\rm d}\mathbf{r}'\frac{n(\mathbf{r}')}{\mid \mathbf{r}-\mathbf{r}' \mid} \;, \\
V_{{\rm xc}\delta} &= \frac{\partial[n e_{\rm xc}(n_\delta,\gamma)]}{\partial n_\delta} - \frac{e}{n}\mathbf{j}_p\cdot\mathbf{A}_{\rm xc} \;,
\end{aligned} \tag{11}$$

where we have dropped the arguments $\mathbf{r}$. The total canonical angular momentum of the solution is defined as

$$L_z = \sum_{i\delta} f_{i\delta}\langle\Psi_{i\delta} \mid \hat{l}_z \mid \Psi_{i\delta}\rangle \tag{12}$$

$$= m^* \int {\rm d}\mathbf{r}\; [x j_{py}(\mathbf{r}) - y j_{px}(\mathbf{r})] \;. \tag{13}$$

3 Computational method

We use a plane-wave basis

$$\varphi_{\mathbf{k}} = \frac{1}{L}{\rm e}^{i\mathbf{k}\cdot\mathbf{r}} \;, \tag{14}$$

with $\mathbf{k} = \frac{2\pi}{L}(\eta_1, \eta_2)$ and $\eta_{1,2} = -\kappa, -\kappa+1, \ldots, \kappa$ to solve the single-particle Kohn–Sham equation (10) at each iteration. Here L is the side length of the square calculation box and κ the cutoff index determining the number of plane waves used. For the corresponding equidistant space lattice of the box, we use $4\kappa+1$ points per axis. Consequently, the Hamiltonian matrix is completely filled, and the the diagonalization basis set (14) is used in the best possible way.

We start the calculations by putting initial guesses for $\boldsymbol{\mathcal{A}}(\mathbf{r})$ and $\mathcal{V}_\delta(\mathbf{r})$ in the space lattice points. We usually set $\boldsymbol{\mathcal{A}} = 0$ and use square well potentials with suitable size and

depth and various shapes for $\mathcal{V}_\delta$. We add small random perturbations to the initial potentials to help the system to find solutions with broken symmetries. Using a fast Fourier transform (FFT) the initial potentials are expanded in the plane wave basis. The Hamiltonian matrices in the basis set (14) are now calculated and diagonalized for up- and down-spin electrons, respectively.

After the diagonalization, the FFT is again used to obtain the eigenstates $\Psi_{i\delta}(\mathbf{r})$ and their derivatives in the space lattice points. From these, the particle densities $n_\delta(\mathbf{r})$, the paramagnetic current density $\mathbf{j}_p(\mathbf{r})$, and vorticity $\gamma(\mathbf{r})$ are determined. Then the new potentials $\mathcal{A}(\mathbf{r})$ and $\mathcal{V}_\delta(\mathbf{r})$ have to be set for the next iteration. It is impossible, however, to calculate the quantity $\mathbf{A}_{\rm xc}$ directly from (11). Due to numerical inaccuracies in areas where the electron density approaches zero, the term $1/n$ diverges faster than the partial derivatives of $\partial[ne_{\rm xc}(n_\delta,\gamma)]/\partial\gamma$ decreases, producing insensibly large values for $\mathbf{A}_{\rm xc}$.

Another problem arises at the edge regions of the dot. Even in areas where the electron density is large enough to generate correct values for $\mathbf{A}_{\rm xc}$, when (11) is used, the function is usually changing rapidly in the finite space lattice used in the calculations. This leads to problems in the convergence process.

We could stabilize the behavior of $\mathbf{A}_{\rm xc}$ on the edge areas of the dot by using the following convoluted form instead of (11):

$$\begin{aligned} eA_{{\rm xc}x} &= \frac{\partial\widetilde{e}_{\rm xc}}{\partial\gamma}\frac{\partial}{\partial y}\ln(n)+\frac{\partial}{\partial y}\frac{\partial\widetilde{e}_{\rm xc}}{\partial\gamma}\,,\\ eA_{{\rm xc}y} &= -\frac{\partial\widetilde{e}_{\rm xc}}{\partial\gamma}\frac{\partial}{\partial x}\ln(n)-\frac{\partial}{\partial x}\frac{\partial\widetilde{e}_{\rm xc}}{\partial\gamma}\,, \end{aligned} \tag{15}$$

where

$$\frac{\partial\widetilde{e}_{\rm xc}}{\partial\gamma}=\int {\rm d}\gamma'\frac{\gamma'-\gamma}{\sqrt{2\pi}\Delta^3}{\rm e}^{\frac{-(\gamma'-\gamma)^2}{2\Delta^2}}e_{\rm xc}(n_\delta,\gamma')\,. \tag{16}$$

Here, (15) is analytically equivalent to the original form in (11), but avoids the divergence of the $1/n$ term in the low-density regions. In addition, $e_{\rm xc}$ is Gaussian-convoluted with respect to the vorticity and now assigned the symbol $\widetilde{e}_{\rm xc}$. The value of the convolution parameter Δ is chosen such that it drains the dependence of $\widetilde{e}_{\rm xc}$ on γ for very low particle densities, but is of negligible effect otherwise. The convolution integral is done numerically. To apply (15) to $\mathbf{A}_{\rm xc}$, we again use the FFT for the derivatives. First, the values of $\ln(n)$ and $\frac{\partial\widetilde{e}_{\rm xc}}{\partial\gamma}$ are calculated in the space lattice points and then expanded in the plane-wave basis. The derivative is taken analytically and turned back into the space lattice. To calculate the scalar Hartree potential, we also use the plane-wave expansion.

Once the new potentials $\mathcal{A}$ and $\mathcal{V}_\delta$ are at one's disposal, one should not rush into the second iteration immediately, especially because the long-range Coulomb interaction makes the system very unstable against enhancing density oscillations from iteration to iteration. To stabilize the convergence behavior, one uses the mixing formula

$$\mathcal{V}_{i+1}=(1-a_1+a_2)\mathcal{V}_i-a_2\mathcal{V}_{i-1}+a_1\mathcal{V}\,, \tag{17}$$

for all potentials $\mathcal{A}$ and $\mathcal{V}_\delta$. Here $\mathcal{V}_{i+1}$ is the potential to be used on the next iteration, and $\mathcal{V}_i$ and $\mathcal{V}_{i-1}$ analogously are the potentials for the current and previous iteration, respectively. $\mathcal{V}$ is the pure new potential discussed above. For the parameters a_1 and a_2 we typically have used values of 0.02 and 0.70. The parameter a_1 determines approximately how fast the potential is moving towards the new potential $\mathcal{V}$, and a_2 determines the inertia of the solution. The above parameter values indicate slow speed with high inertia. Even if the suggested potential suddenly changes to something completely different, the solution continues on its old path for a while. This is the desired behavior in the case of level crossings, for example, and also makes the final approach to the converged solution faster. For full convergence, however, several hundred iterations are usually needed.

The interpolation formula for $e_{\rm xc}$ is given in terms of total particle density n, spin polarization $\xi=(n_\uparrow-n_\downarrow)/n$, and filling factor $\nu=2\pi\hbar n/eB$, where B is replaced by $m^*\mid\gamma\mid/e$ for CSDFT (9). For now, we have used

$$e_{\rm xc}(n,\xi,\nu)=e_{\rm xc}^{\infty}(n)e^{-f(\nu)}+e_{\rm xc}^{\rm TC}(n,\xi)(1-e^{-f(\nu)}) \tag{18}$$

where $f(\nu)=1.5\nu+7\nu^4$. This form interpolates between the infinite magnetic field limit

$$e_{\rm xc}^{\infty}(n)=-0.782\sqrt{2\pi ne^2}/4\pi\epsilon_0\epsilon \tag{19}$$

and the zero field limit $e_{\rm xc}^{\rm TC}(n,\xi)$ of Tanatar and Ceperly [10] generalized for intermediate polarizations [7]. For $\nu<0.9$, the interpolation (18) follows closely the results of Fano and Ortolani [11] for polarized electrons in the lowest Landau level, and saturates quickly to a zero field result for $\nu>1$.

4 Results

As an example, we consider a typical 10-electron quantum dot in a GaAs heterostructure, e.g., $m^*=0.067m_{\rm e}$, $\epsilon=12.4$, and the spherical harmonic confining potential $\hbar\omega_0=3\,{\rm meV}$.

For $B=3.4\,{\rm T}$, the total charge density (see Fig. 1a) is rotationally symmetric, forming the so-called maximum-density droplet [12]. The corresponding current density $\mathbf{j}(\mathbf{r})$ is plotted as a function of the spatial coordinates $\mathbf{r}=(x,y)$ in atomic units in the vector diagram in Fig. 1b. (The maximum length along each axis corresponds to 14.4 a.u.). Two rotationally symmetric current loops circulating in opposite directions are seen. When the magnetic field is increased, the charge density in the internal coordinates breaks rotational symmetry, forming a bumpy structure (see Fig. 2a), as has also been observed in the Hartree–Fock calculations of Müller and Koonin [9]. Here, the current density also shows a broken symmetry, forming vortex-like structures which have their centers at the maxima of the charge density (see Fig. 2b).

Similar results were found for other electron numbers, and the general scenario seems to be that right

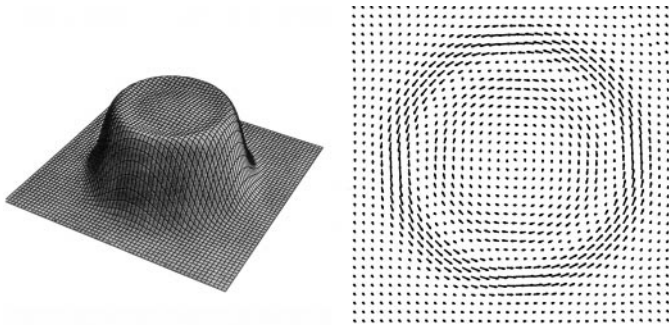

Fig. 1. Total density $n(\mathbf{r})$ (a) and current density $\mathbf{j}(\mathbf{r})$ (b) for a quantum dot with 10 electrons and $r_s = 1.7$ a.u. at $B = 3.4$ T, which forms a maximum-density droplet [12].

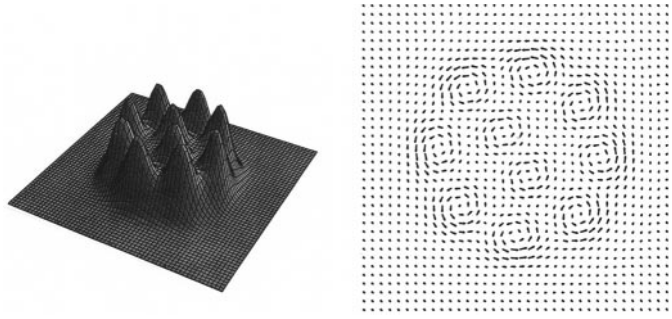

Fig. 2. As in Fig. 1, but for $B = 6.9$ T. In such strong magnetic fields, solutions with broken rotational symmetry exist.

after the dot becomes fully polarized, the density profile has perfect azimuthal symmetry. The density inside the maximum-density droplet is nearly constant, with only a small wiggle right at the edge, where it continuously drops to zero. The orbital angular momentum then equals $L_z = \frac{1}{2}N(N-1)$, corresponding to the occupation of all the (spin-polarized) orbitals with $0 \leq l \leq N-1$. Increasing the field strength leads to a reconstruction of the density distribution inside the dot: Some electrons are promoted to orbitals with higher angular momentum, leaving some of the lower angular momentum states unoccupied. This results in an overall bumpy electron density, as shown in Fig. 2a. Within Hartree–Fock calculations assuming rotational symmetry, edge reconstruction was first found by Chamon an Wen [13]. The edge regions, however, also have broken rotational symmetry [14] in the internal coordinate system, and are the precursors of the bumpy states.

5 Conclusions

We have applied CSDFT to circular quantum dots in large magnetic fields and found that the maximum-density droplet develops into a state with broken rotational symmetry, in agreement with the results of [9]. We point out that calculations restricted to azimuthal symmetry cannot account for the rich variety of density distributions in the internal coordinates. We finally mentioned that in larger circular dots, edge states, formed as suggested by Chamon and Wen [13], have a broken radial symmetry [14].

We thank Ben Mottelson for many inspiring comments and discussions, and acknowledge helpful correspondence with D.G. Austing. This work was supported by the Academy of Finland and the TMR program of the European community under contract ERBFMBICT972405.

References

1. L.P. Kouwenhoven *et al.*: *Electron transport in quantum dots*, in *Proceedings of the Advanced Study Institute on Mesoscopic Electron Transport, 1997*, ed. by L.L. Sohn, L.P. Kouwenhoven, G. Schön
2. M.I. Lubin, O. Heinonen, M.D. Johnson: Phys. Rev. B **56**, 10 373 (1997)
3. O. Heinonen, J.M. Kinaret, M.D. Johnson: [Cond-Mat/97712168]
4. M. Ferconi, M.R. Geller, G. Vignale: Phys. Rev. B **52**, 16 357 (1995)
5. S. Tarucha, D.G. Austing, T. Honda, R.J. van der Hage, L.P. Kouwenhoven: Phys. Rev. Lett. **77**, 3613 (1996)
6. D.G. Austing *et al.*: Jpn. J. Appl. Phys. (1998) (in print)
7. M. Koskinen, M. Manninen, S.M. Reimann: Phys. Rev. Lett. **79**, 1817 (1997)
8. G. Vignale, M. Rasolt: Phys. Rev. B **37**, 10 685 (1988)
9. H.-M. Müller, S.E. Koonin: Phys. Rev. B **54**, 14 532 (1996)
10. B. Tanatar, D.M. Ceperley: Phys. Rev. B **39**, 5005 (1989)
11. G. Fano, F. Ortolani: Phys. Rev. B **37**, 8179 (1987)
12. A.H. McDonald, S.R. Eric Yang, M.D. Jonson: Aust. J. Phys. **46**, 345 (1993)
13. C. de C. Chamon, X.G. Wen: Phys. Rev. **49**, 8227 (1994)
14. S.M. Reimann, M. Koskinen, M. Manninen, B.R. Mottelson: [cond-mat/9904067]